A Novel Phase-Locking-Free Phase Sensitive Amplifier based Regenerator

Kjøller, Niels-Kristian; Røge, Kasper Meldgaard; Guan, Pengyu; Mulvad, Hans Christian Hansen; Galili, Michael; Oxenløwe, Leif Katsuo

Published in:
Journal of Lightwave Technology

Link to article, DOI:
10.1109/JLT.2015.2482122

Publication date:
2016

Document Version
Peer reviewed version

A Novel Phase-Locking-Free Phase Sensitive Amplifier based Regenerator

Niels-Kristian Kjøller, Kasper Meldgaard Røge, Pengyu Guan, Hans Christian Hansen Mulvad, Michael Galili and Leif Katsuo Oxenløwe

***Abstract*—We propose a scheme for phase regeneration of optical binary phase-shift keying (BPSK) data signals based on phase sensitive amplification without active phase-locking. A delay interferometer (DI) is used to convert a BPSK signal impaired by noise to an amplitude modulated signal followed by cross-phase modulation (XPM) in a highly nonlinear fiber (HNLF) which transfers the data modulation from the amplitude modulated signal to the phase of a locally generated carrier. By placing the HNLF in a loop a stable phase relation is maintained relative to a set of counter propagating locally generated phase-locked pumps. As a result, active phase-stabilization is avoided. A proof-of-principle experiment is carried out with a dual-pump degenerate phase sensitive amplifier (PSA), demonstrating regeneration for a 10 Gb/s non-return-to-zero differential BPSK (NRZ-DPSK) data signal degraded by a sinusoidal phase-noise tone. Receiver sensitivity improvements of 3.5 dB are achieved at a bit-error-rate (BER) of 10^{-9}. Additionally, numerical simulations are performed comparing the idealized regenerator performance in the presence of sinusoidal phase modulation as well as Gaussian phase-noise.**

***Index Terms*—Cross-phase modulation, nonlinear optical signal processing, optical fiber communication, phase locked loops, phase regeneration, phase sensitive amplification.**

I. Introduction

OPTICAL signals propagating in fiber-optic transmission systems are impaired by noise which accumulates as a consequence of amplified spontaneous emission (ASE) from optical amplifiers and nonlinear optical effects in the transmission fiber. Noise suppression by optical data regenerators represents a potential for significantly increasing the capacity and reach of optical fiber communication links. In the last decades optical communication systems have migrated from binary intensity-modulated on-off keying (OOK) to phase-modulated data formats such as binary phase-shift keying (BPSK) and quadrature phase-shift keying (QPSK), which offer several advantages over OOK such as better receiver sensitivity and higher spectral efficiency, respectively. Phase sensitive amplification, a technique based on parametric mixing between waves in a nonlinear optical medium, have proved particularly promising for regeneration of such phase-modulated data formats, and optical phase regeneration has been demonstrated not only for BPSK [1–3], but also for multilevel formats such as QPSK [4] and star-8QAM [5].

Phase sensitive amplification requires a stable phase relation between the phase modulated signal and the involved pumps at the input of the nonlinear medium [6]. For practical ('black-box') applications the pumps have to be generated locally at the processing stage. A suitable set of coherent waves can be generated in a four-wave mixing (FWM) pre-stage as in [2, 4]. FWM between the data signal and a local continuous wave (CW) pump in a highly nonlinear fiber (HNLF) is used to generate a second pump which inherits its phase from the data signal and the other pump. Subsequently, the original data signal is combined with the two phase-locked pumps and sent to the PSA. However, in this approach the separate optical paths of the signal and pumps necessitate the use of an optoelectronic phase-locked loop (PLL) to compensate for thermal drifts. This turns out to be cumbersome and practically challenging, especially for longer separate path lengths. Solutions not requiring the use of PLLs may thus provide increased long term stability.

In [7, 8] an approach relying on the $\chi^{(2)}$ effects sum- and difference frequency generation in cascaded periodically poled lithium niobate (PPLN) devices is demonstrated for QPSK regeneration. Introducing an additional HNLF-based equalizer unit, the amplitude is also regenerated. This scheme may possibly be extended to higher PSK formats without increasing the number of active components. Furthermore, PPLNs offer high conversion efficiency for low pump power and are compact components. Some challenges with PPLN remain, though, such as the need for accurate temperature control, challenges with obtaining an efficient broad quasi-phase matched (QPM) bandwidth, and in particular the need for controlling the dispersion in the fundamental and the second harmonic wavelength range, i.e. very carefully controlling the group velocity mismatch (GVM) to avoid walk-off based pulse broadening of the harmonic component [9]. The latter imposes a symbol rate limitation on applications, where the full data signal needs to be processed, such as wavelength conversion and regeneration. In contrast, in HNLF one only needs to control the dispersion and associated walk-off in the 1550 nm

This work is supported by the Danish Council for Independent Research (FTP) through the TOR project (grant no. 12-127224). The authors would like to thank OFS Fitel Denmark ApS for providing the HNLF-SPINE fiber.

N. K. Kjøller, K. M. Røge, P. Guan, M. Galili and L. K. Oxenløwe are with the Technical University of Denmark, Department of Photonics Engineering, DK-2800 Kgs. Lyngby, Denmark, (e-mail: niekjol@fotonik.dtu.dk).

H. C. H. Mulvad is with the Optoelectronics Research Centre, University of Southampton, Southampton, SO17 1BJ, U.K.

Color versions of one or more of the figures in this paper are available online at http://ieeexplore.ieee.org.

Digital Object Identifier 10.1109/JLT.201XXXXXXXX

wavelength range, as e.g. allowing for pulse-broadening-less Tbit/s de-multiplexing [10].

In [11] we proposed a novel scheme for PSA based regeneration without any electronic phase locking. This paper is an extension of the conference paper [11]. A stable phase relation is maintained by a passive loop configuration in which the signal and pumps are pre-conditioned for phase sensitive amplification. This is achieved by first using a delay interferometer (DI) to demodulate a BPSK signal impaired by noise to an amplitude modulated signal and subsequently cross-phase modulation (XPM) to modulate the signal onto a locally generated carrier recovering the BPSK modulation. As a result of XPM the signal experiences wavelength conversion. A similar approach to phase regeneration has previously been demonstrated in [12, 13], where instead of regenerating the phase modulated carrier directly an amplitude regenerator such as Mamyshev (see [14]) is used prior to XPM. The Mamyshev regenerator require the input signal to be return-to-zero (RZ) modulated as the scheme relies on self-phase-modulation. The proposed scheme on the other hand is demonstrated for non-return-to-zero (NRZ) and can be extended to RZ signals with few modifications. A variant of the DI, XPM and PSA combination is investigated theoretically in [15]. Here, a one bit DI and XPM in a HNLF are used for data transfer onto a locally generated carrier, prior to regeneration in a PSA using electronic phase stabilization. Locking the pumps to the external data signal is thus circumvented but replaced by the need to lock the local carriers electronically.

The proposed scheme is detailed in the following. After providing a simple analytical comparison between the PSA with the employed optical pre-conditioning principle and an ordinary PSA in Section II, a proof-of-principle experimental demonstration is provided by performing phase-regeneration of an optical 10 Gb/s non-return-to-zero differential BPSK (NRZ-DPSK) signal degraded by a 3.7 - 5.7 GHz sinusoidal phase-noise in Section III. The inherent phase stability of the scheme permits a precise dynamic characterization with a DPSK modulated signal of the full phase sensitive response in the PSA. This is presented in Section IV along with measurements of the BER-performance. Finally, since phase-noise emulation using a single frequency tone does not represent the signal impairments in a real transmission scenario, numerical simulations are included in Section V to compare the regenerator performance to the case of Gaussian phase-noise.

II. Principle of Operation

The main idea of the proposed scheme is to locally generate a suitable set of phase-locked carriers, and transfer the phase modulation of an incoming data signal to one of those carriers, without disturbing the overall phase relationship between the pumps and the data signal carrier. The method used is illustrated in Fig. 1: An optical comb consisting of three phase-locked carriers are used as pumps and signal in a PSA. The incoming BPSK signal is passed through a one bit DI and converted to an amplitude modulated signal. XPM in a HNLF is employed to transfer the data modulation from the amplitude modulated signal to the phase of the central of the phase locked carriers. This is achieved by constructing a fiber loop where the two outer carriers, to be used as PSA pumps, propagate in one direction and the central carrier and the amplitude modulated signal travel in the opposite direction. Equal path lengths ensured by the loop configuration maintains the phase relation, and the output is three phase-locked carriers, one of which is now containing the phase modulated data. For regeneration, the three carriers are then sent to a second HNLF, where phase sensitive amplification regenerates the data modulated on the central carrier. For BPSK, regeneration results from interference between the signal carrier and a phase conjugated FWM idler generated at the signal wavelength, resulting in a step transfer function for the phase, as first proposed in [1]. Potential extension to QPSK signal regeneration could be achieved either by generating a four-level amplitude modulated signal in a single DI or by the use of two parallel DIs and two consecutive XPM stages, with $2\gamma P_{in}L \approx \pi$ and $2\gamma P_{in}L \approx \pi/2$ respectively, as in [16, 13] combined with a PSA suitable for QPSK regeneration such as in [4].

The data thus undergoes three processing steps; DI, XPM and PSA. In Fig. 2 the effect of each step is shown for a simulated pseudo-random bit sequence (PRBS) of length $2^7 - 1$ where each bit is represented by a point in the IQ-plane. At the

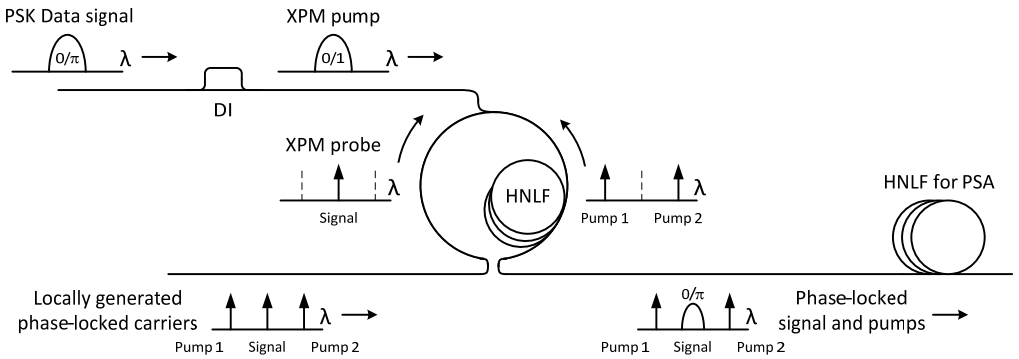

Fig. 1. The general scheme for signal and pump pre-conditioning. A locally generated set of phase locked carriers is to be used as signal and pumps in the PSA. An incoming BPSK modulated signal is converted to an amplitude modulated signal in a DI, and used as XPM pump in the loop. The phase modulation is thus transferred to the signal carrier without disturbing the overall phase relationship between the pumps and the data signal carrier.

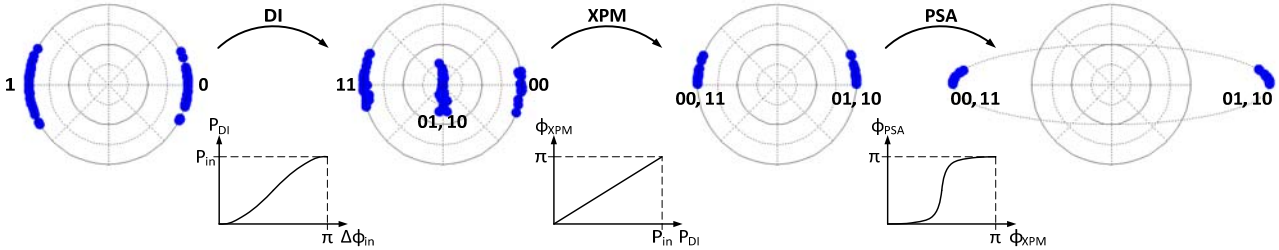

Fig. 2. The three steps of data processing; DI, XPM and PSA. The transfer function of each step (shown below each arrow) is applied to a PRBS with Gaussian phase noise. The DI converts phase modulation to modulation of output power by interfering two consecutive bits. XPM converts modulation of the signal power to phase modulation, either 0 or π, of the data carrier. Finally, the PSA regenerates the phase modulation by squeezing the phase.

input, Gaussian distributed noise is added to the phase of each bit and the theoretical transfer function for each step is applied to the constellation diagram in sequence. Assuming constant amplitude (a), the DI converts phase modulation (φ) to modulation of output power (P) according to [17]

$$P_{DI} = P_{in}\cos^2\tfrac{1}{2}(\varphi_1 - \varphi_2), \quad (1)$$

by interfering two consecutive bits having phases φ_1 and φ_2 and input power P_{in}. This process alters the data pattern now encoded on the signal amplitude. The pattern conversion can be reversed either by precoding in the transmitter or by a decoder in the receiver in the electronic domain [18, 19]. Second, the XPM converts modulation of the signal power to phase modulation of the central carrier as [20]

$$\varphi_{XPM} = 2\gamma P_{DI} L, \quad (2)$$

with γ and L being the nonlinearity coefficient and length of the HNLF used for XPM. To ensure that the carrier is modulated with either 0 or π, the fiber parameters and input power should be chosen so that $2\gamma P_{in} L \approx \pi$. Notice in Fig. 2 how the XPM output is limited to $0 \le \varphi \le \pi$ which is the case when $2\gamma P_{in} L = \pi$. Finally, the PSA regenerates the phase modulation of the central carrier. In a PSA based on degenerate four-wave mixing, the in-phase component I of the electric field experiences a gain g while the quadrature component Q experiences a de-amplification of $1/g$ [6] and the resulting phase and amplitude of the output signal may be written in terms of φ_{XPM} and a_{XPM} as

$$\tan\varphi_{PSA} = g^{-2}\tan\varphi_{XPM}, \quad (3)$$

$$a_{PSA} = \frac{a_{XPM}}{\sqrt{2}}\sqrt{(g^2+g^{-2}) + (g^2-g^{-2})\cos(2\varphi_{XPM})}. \quad (4)$$

Here g is the gain of the PSA. As seen from Fig. 2, the phase sensitive amplification result in a squeezing of the constellation points towards 0 and π. It should be noted that the above analysis provides only a description of the key operating principle targeted in the regenerator. It does not provide a full description of the system.

Fig. 3 shows the resulting transfer functions (DI+XPM+PSA) for the data modulation in the ideal system compared to that of using only a PSA, for three different phase sensitive extinction ratios (PSERs) – defined as the ratio between the maximum and minimum phase sensitive gain. The output phase, investigated in Fig. 3(a), is a step-like function alternating between the two values 0 and π due to (2). The

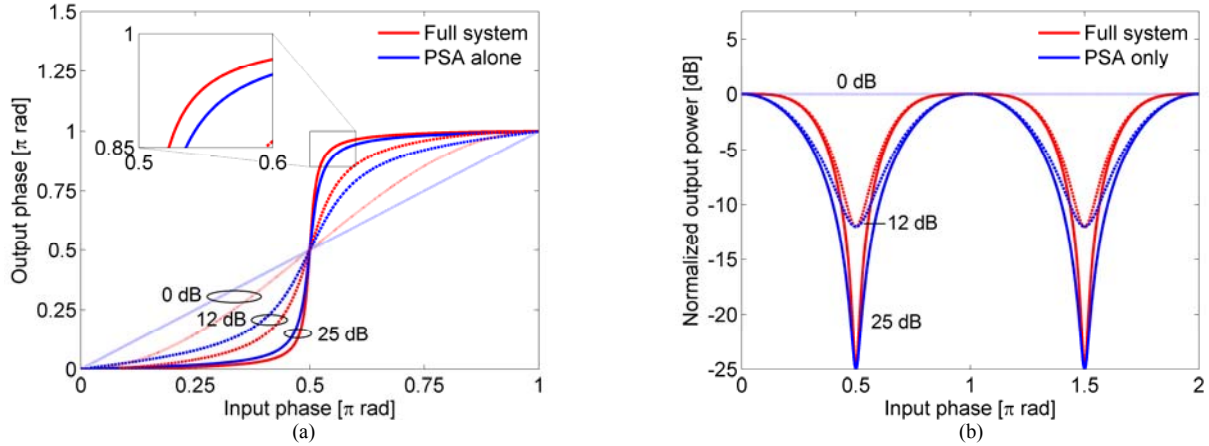

Fig. 3. Theoretical transfer functions for the data modulation in an ideal system, compared to that of an ideal PSA, for PSERs of 0 dB (dotted), 12 dB (dashed) and 25 dB (solid). (g = 1, 2.0 and 4.2 respectively.). (a) Phase-to-phase and (b) phase-to-power.

output power, see Fig. 3(b), resembles a sinusoid with minima at $\pi/2$ and $3\pi/2$ but with flat areas of equal amplification around 0 and π. In Fig. 3(a) the phase-to-phase transfer functions are compared. In the case of PSER = 0 dB (g = 1) the PSA is not regenerating, and the transfer function of the PSA alone (blue) is a straight line. However, the transfer function of the full system (red) shows signs of regeneration, due to the transfer function of the DI. For PSER = 12 dB (g = 2.0) the transfer function is mostly influenced by the PSA albeit an improvement is still seen over the case of PSA alone. As the PSER is increased, the transfer function of the full system converges to an ideal staircase slightly faster than that of the PSA alone but is strongly dominated by the properties of the PSA for PSERs above ~20 dB. In Fig. 3(b) the phase-to-power transfer functions are compared. Again, for PSER = 0 dB the PSA is not regenerating and output power is constant for both cases. For PSER = 12 dB the regeneration of the DI is evident: The DI and XPM steps combine to yield a slight squeezing of the constellation points towards 0 and π without changing the amplitude as evident in Fig. 2. As a result, the transfer function of the full system shows flat areas of equal amplification around 0 and π not present for the PSA alone. Thus, for values of φ close to 0 or π the constellation points are squeezed towards 0 or π with equal level of amplification. Minima are at $\pi/2$ and $3\pi/2$ and constellation points around the middle between 0 or π are de-amplified by the regenerator to the same minima as the case of PSA alone. An increase to PSER = 25 dB is seen not to affect the line-shape of the transfer function; only a scaling occurs to yield the 25 dB ratio between maximum and minimum.

In the above discussion, only noise on the phase of the data modulated signal is considered. Likewise, in the following sections only regeneration of phase noise impaired signals is investigated experimentally. However, considering (1) – (2) it is clear that any amplitude noise on the data signal will be converted into phase noise on the π-bits of the XPM output. This is clearly seen in Fig. 4, where the system output is compared to the case of PSA alone for an input PRBS of length $2^7 - 1$ impaired by both phase and amplitude noise in the form of equal amounts of noise on the I and Q components. Furthermore, due to the mixing of consecutive bits in the DI the upper limit on the applicable phase noise strength is reduced, as each bit of the output of the DI carry the combined noise from two consecutive bits. As can be seen from Fig. 3(a) and 3(b), the proposed scheme is, in theory, slightly better than an ordinary PSA in the absence of amplitude noise. Numerical simulations based on (1) – (4) show that some amount of amplitude noise can be handled by the system, in the case of phase noise being dominant. Comparable levels of noise on the I and Q components will however reduce the overall performance below that of an ordinary PSA as seen in Fig. 4. Regeneration will still take place, though, for sufficiently high values of g.

III. Experimental Demonstration for DPSK

The regenerator is demonstrated experimentally for a dual-pump degenerate PSA, as illustrated in Fig. 5, but is not limited to this specific type of PSA in general. Three phase-locked carriers are generated using four wave mixing, by injecting two CW signals at 1544 nm (S) and 1542.7 nm (P1) from narrow linewidth (<100 kHz) external cavity lasers into a 200 m HNLF (γ: 4 W^{-1}·km^{-1}, dispersion D: 0.21 ps/(nm·km), dispersion slope $dD/d\lambda$: 0.053 ps/(nm^2·km) at 1550 nm, and zero dispersion wavelength λ_0: 1554 nm), to yield an idler at 1545.3 nm (P2). The phase of the generated idler obeys [21]

$$\varphi_{P1} + \varphi_{P2} - 2\varphi_S = 0, \tag{5}$$

which guarantees a stable phase relation. The three co-polarized carriers were aligned at 45º with respect to the primary polarization axis of a polarization maintaining fiber (PMF). The total birefringence of the PMF was matched to the spacing of the three carrier waves, resulting in a 90° rotation of the polarization of S relative to P1 and P2. This allows using a polarizing beam splitter (PBS) to send the carrier waves S and P1, P2 in opposite directions inside a loop containing 500 m of HNLF (γ: 11.8 W^{-1}·km^{-1}, D: –0.00723 ps/(nm·km), $dD/d\lambda$: 0.01853 ps/(nm^2·km) at 1550 nm, λ_0: 1550.39 nm).

An NRZ-DPSK data signal is generated by modulating a CW at 1560 nm (linewidth <100 kHz) with a 10-Gbit/s pseudo-random bit sequence (PRBS) of length $2^{31} - 1$ using a standard Mach-Zender modulator (MZM). Phase noise was emulated by adding sinusoidal phase modulation to the DPSK signal using a phase modulator (PM) driven by a single RF tone generated from an unsynchronized RF source. To generate a pump for the XPM process, the phase modulated data signal is converted to an amplitude modulated signal in a 1 bit (100 ps) fiber DI and amplified using an erbium doped fiber amplifier (EDFA). The XPM pump is coupled into the loop in the same direction as S, and by carefully adjusting the XPM pump power, the phase of S is encoded with either 0 or π. The counter-propagating pumps encounter several thousand bits in the 500 m HNLF, and experience only a constant phase offset. After the HNLF, a 5-nm optical band pass filter (OBPF) is used

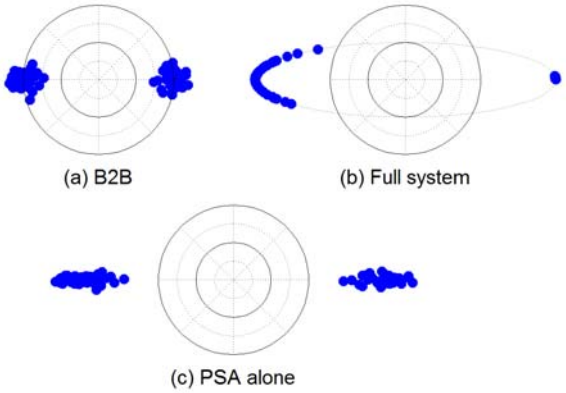

Fig. 4. Regenerator output in the presence of both phase and amplitude noise compared to the case of a PSA alone. (a) Input constellation, (b) regenerator output and (c) output in case of the PSA alone.

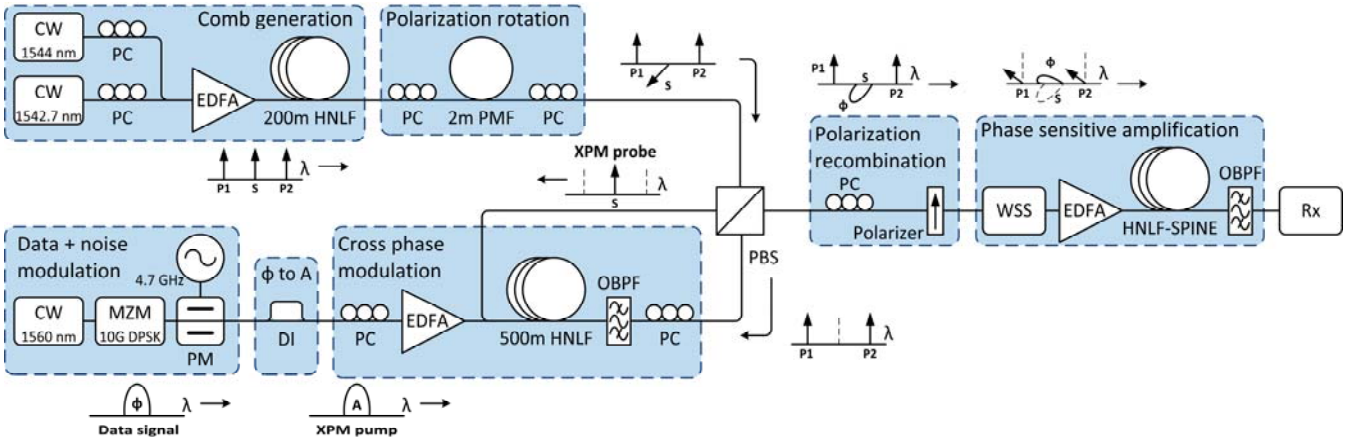

Fig. 5. The experimental setup for the phase-locking-free dual-pump degenerate PSA based regenerator. FWM between two CW signals are used for comb generation and a matched PMF is used to rotate the polarization of the signal carrier S relative to the pumps P1, P2 enabling separation in a PBS. XPM between S and the DI-demodulated DPSK signal takes place in a 500 m HNLF, and after the loop P1, P2 and S are recombined using a polarizer. PSA between the phase-locked carriers takes place in a 250 m HNLF-SPINE, thus regenerating the data modulated carrier S.

to select only the three original phase-locked carriers. Using a polarization controller (PC) the two pumps P1, P2 and the now DPSK modulated signal S are aligned to exit the loop by the remaining port of the PBS. At this point, S is still orthogonally polarized to P1 and P2, and a polarizer is used to project them onto the same plane of polarization, causing a 3-dB loss in power for all waves.

An optical processor (Finisar Waveshaper 4000 – WSS) is used to equalize the pumps, remove out of band noise and adjust power and phase of S relative to the pumps P1 and P2, in order to optimize the PSA performance. The signal S and pumps P1, P2 are then launched into a 250 m strained HNLF with stable phase-matching for improved nonlinear efficiency (HNLF-SPINE, γ: 9.4 $W^{-1}{\cdot}km^{-1}$, D: 0.45 ps/(nm·km), $dD/d\lambda$: 0.070 ps/(nm^2·km), λ_0: 1544 nm) with an SBS threshold of 27.5 dBm, here defined as the power level at which the SBS reflected light power is equal to 10% of the input power. After phase sensitive amplification in the HNLF-SPINE, P1 and P2 are removed using a tunable flat-top OBPF, and the output is sent to a pre-amplified DPSK receiver (Rx), comprising a 1 bit fiber DI followed by a balanced photodiode and an electrical low-pass filter with a cut-off at 7.5 GHz, for bit-error-ratio (BER) testing.

IV. Experimental Results

At the output of the HNLF-SPINE, the signal and pump powers are measured using an optical spectrum analyzer as the phase of the data modulated signal S is swept relative to the phases of the pumps P1, P2 using the optical processor. Due to the inherent phase stability of this scheme, a precise dynamic characterization, i.e. with a DPSK modulated signal, of the full phase sensitive response in the PSA is made possible.

Static characterizations of the phase sensitive response are reported in Fig. 6(a) for increasing levels of total input power. A strong phase sensitive interaction is witnessed by a maximum PSER of 24.8 dB seen for a total power of 27.8 dBm launched

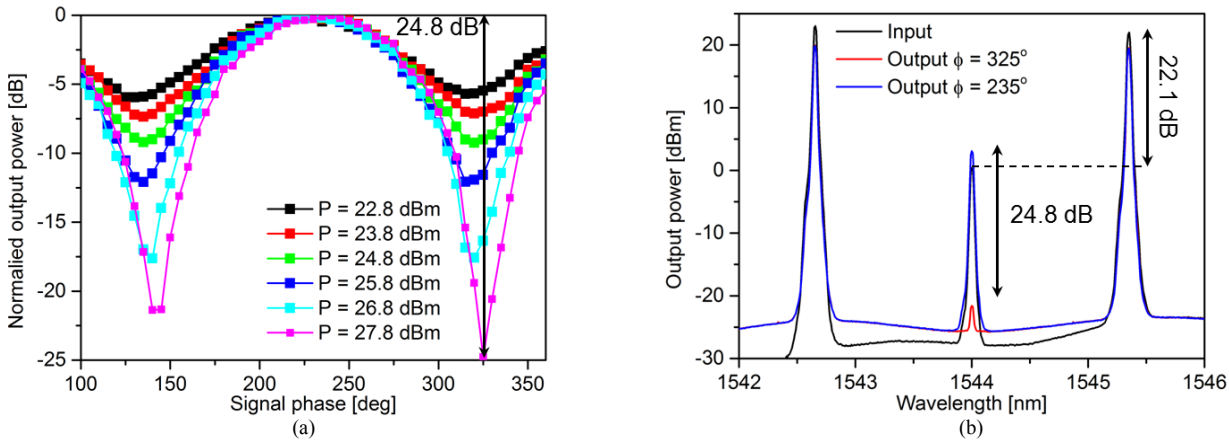

Fig. 6. Characterization of static operation of the PSA. (a) Normalized phase sensitive gain of the signal as a function of signal phase for increasing levels of total power P. (b) Spectra at the input and output of the HNLF-SPINE for maximum and minimum output signal power for a total input power of 27.8 dBm.

into the HNLF-SPINE and a pump to signal power ratio of 22.1 dB. The phase sensitive response is clearly periodic with a period of 180°, and in resemblance of the theoretical phase-to-power transfer function of a PSA in Fig. 3(b) (blue), indicating a stable phase relation between the carriers and the desired interaction between the signal and the phase conjugated FWM idler. The input spectrum and output spectra for maximum amplification (ϕ = 235°) and deamplification (ϕ = 325°) are reported in Fig. 6(b), showing the 24.8 dB ratio between the maximum and minimum phase sensitive gain.

Dynamic characterizations of the phase sensitive response are reported in Fig. 7(a) and comparison between the input spectrum and output spectra for maximum amplification (ϕ = 205°) and de-amplification (ϕ = 295°) are reported in Fig. 7(b). Comparing to the static characterization, the power of the signal has been increased relative to the pumps in order to increase the ONSR. As a result, the PSA is operated in mild saturation, as can be seen by the power fluctuation of the pumps, causing a decreased phase sensitive gain. At a total input power of 28.8 dBm and a pump to signal power ratio of 9.2 dB the resulting PSER is 12.2 dB, as is evident in both Fig. 7(a) and (b). Saturation can be reduced by reducing the signal power, at the cost of signal OSNR. However, operation at lower levels of OSNR was observed to reduce the BER performance of the regenerator.

For BER testing, phase noise is added as described above and the modulation index and the frequency of the noise tone are varied to investigate the performance of the regenerator under different operating conditions. The BER of the signal is measured back-to-back (B2B), as well as before and after the PSA (labelled After XPM and After PSA, respectively), for no degradation as well as for noise tone frequencies of 3.7 GHz, 4.7 GHz and 5.7 GHz. The frequencies were chosen high enough to yield significant bit-to-bit changes while staying below the cut-off frequency of the electrical low-pass filter at the receiver. For the reported measurements, the modulation index of the phase noise (defined as $m = \pi V_{pp}/2V_\pi$, with V_{pp} being the peak-to-peak voltage of the driving signal and V_π being the half-wave voltage of the phase modulator) is fixed at 0.56, corresponding to a peak-to-peak phase distortion of 1.12 rad or 64°.

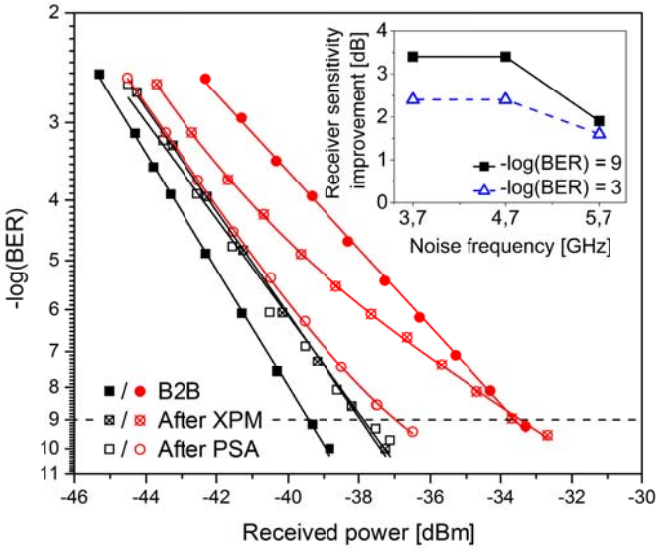

Fig. 8. BER as a function of received power B2B (solid), after XPM (crossed) and after PSA (open), with (red) and without (black) 4.7 GHz phase noise. Inset: Improvement in receiver sensitivity as a function of noise frequency at BER = 10^{-3} (blue) and BER = 10^{-9} (black).

The resulting BER curves are shown in Fig. 8 for a noise frequency of 4.7 GHz. In the absence of added noise, the process of transferring the phase modulation of the data signal to the central of the three phase locked carriers (by DI and XPM) results in a power penalty of around 1.5 dB compared to the B2B reference, while the added penalty of the PSA is insignificant (<0.1 dB). When phase noise is added to the signal, the regeneration (here defined as the ability to improve receiver sensitivity) abilities of the DI is confirmed to be

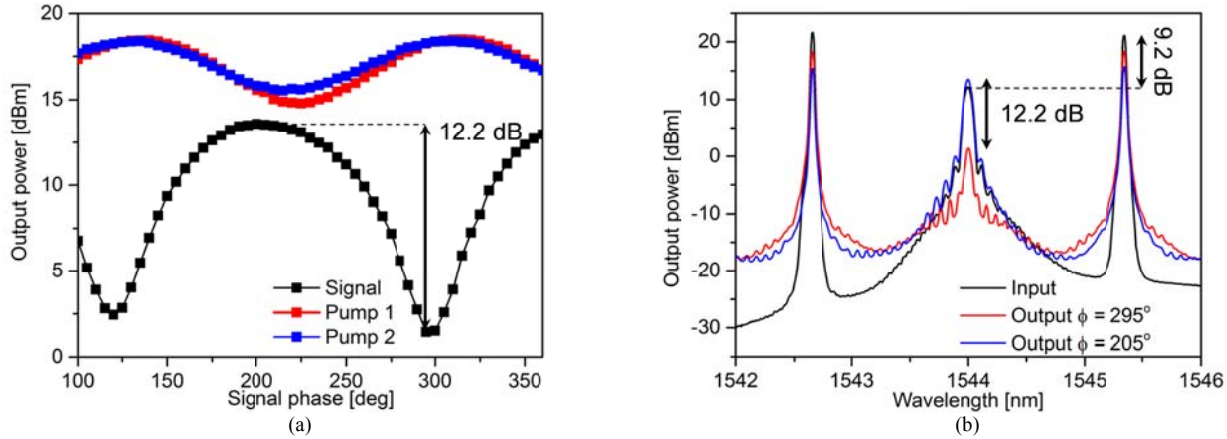

Fig. 7. Characterization of dynamic operation of the PSA. (a) Phase sensitive gain of the signal and pumps as a function of signal phase with 10 Gbit/s data modulation and no noise added. (b) Spectra at the input and output of the HNLF-SPINE for maximum and minimum output signal power (10 Gbit/s data, no noise added). Comparing to the static characterization, notice the reduced phase sensitive extinction ratio due to an increased relative signal power resulting in a mild saturation of the pumps.

significant at low receiver power levels, but diminishing at a BER = 10^{-9}. After the PSA however, the output shows improved receiver sensitivity of 3.5 dB at BER = 10^{-9}, decreasing the power penalty to within 1 dB of the curve measured without added phase noise.

Similar trends are seen for noise tone frequencies of 3.7 GHz, 5.7 GHz, and the improvement in receiver sensitivity is shown as a function of noise tone frequency at BER = 10^{-3} and BER = 10^{-9} in Fig. 8(inset). A reduced degree of regeneration can be seen for a noise tone frequency of 5.7 GHz, and the improvement in receiver sensitivity is only 2.0 dB at BER = 10^{-9}. This behavior may be explained from the roll-off of the electrical low-pass filter in the receiver. For the particular filter we measured a roll-off of the filter transfer function which attenuates the 5.7 GHz noise tone. This partially compensates for the degradation measured B2B caused by the added phase noise. At the regenerator output, however, the measured BER curves are mainly limited by the penalty inherent to the regenerator. As can be seen from Fig. 8, even with no input noise a penalty of 1.5 dB is incurred at the regenerator output. As a result, the output penalty is almost the same for all three investigated noise tone frequencies and a reduction in receiver penalty improvement for 5.7 GHz results from the reduction in B2B penalty.

V. Numerical Simulations

As described above, phase noise was emulated experimentally by adding sinusoidal phase modulation to the DPSK signal. For each bit in the bit-sequence, this can be represented by the addition of a phase error $\delta\varphi$ with a sinusoidal probability density function [22]

$$p_S(\delta\varphi) = \frac{1}{\pi\,\delta\varphi_{max}\sqrt{1-(\delta\varphi/\delta\varphi_{max})^2}}, \qquad (6)$$

with $\pm\delta\varphi_{max}$ being the maximum/minimum value of the modulation, reached for a driving voltage equal to $\pm V_{pp}/2$. However, in optical fiber communication systems, the main noise source is the amplified spontaneous-emission (ASE) noise generated by optical amplifiers. ASE noise can be adequately modeled as a Gaussian stochastic process, as the cumulative effect of many small events due to the Central Limit Theorem [23, 24]. In the small noise limit, the distribution of phase noise converges to a Gaussian with zero mean [25] and a more realistic distribution is thus given by

$$p_G(\delta\varphi) = \frac{1}{\sqrt{2\pi\sigma^2}}\exp\left(-\frac{(\delta\varphi)^2}{2\sigma^2}\right), \qquad (7)$$

where σ^2 is the variance of the distribution.

The sinusoidal phase emulation does not resemble the Gaussian distribution. The effect of Gaussian distributed phase noise on the regenerator performance was investigated numerically based on an ideal implementation of the regenerator, purely governed by the analytical transfer functions (1) – (4). Each bit of a PRBS is represented as a

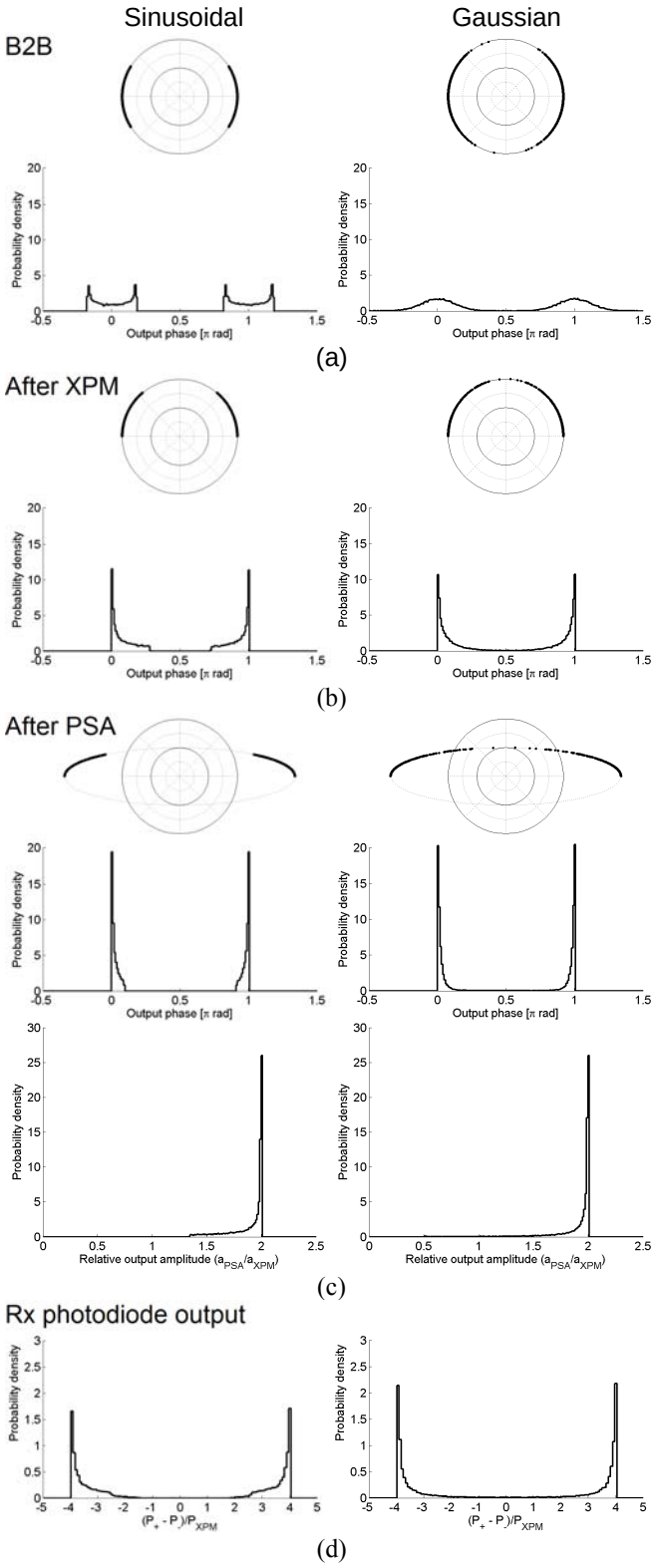

Fig. 9. Simulated regenerator performance in the presence of phase noise with a sinusoidal (left) and a Gaussian distribution (right). The constellation and the sampled phase-value distribution are shown for both noise types at the input (a), after XPM (b) and at the output (c). At the output, the sampled amplitude-value distribution is shown as well. The sampled distribution of the balanced photodiode output is shown in (d).

phasor of phase 0 or π which is then degraded by a random error $\delta\varphi$ drawn from one of the two distributions (6) and (7), for noise levels corresponding to different modulation indices and propagated through the system. Note that in the following simulations, the modulation index is generally expressed as $m = \sqrt{2}\pi V_{RMS}/V_\pi$ where V_{RMS} is the root-mean-square voltage. For a sinusoidal modulation, this reduces to the previously used expression $m = \pi V_{pp}/2V_\pi$. For a Gaussian noise distribution, V_{RMS} is the driving voltage corresponding to a phase shift of σ. For the simulations we choose the amplitude of the input signal and the HNLF parameters such that $2\gamma P_{in} L = \pi$ for the XPM stage, and assume a gain of $g = 2$ in the PSA which corresponds to PSER = 12 dB as was the case for both the dynamic characterization and the BER testing of the previous section.

We investigate how the emulated phase noise is re-distributed when passing through the regenerator, and how this compares to the more realistic Gaussian phase noise. Fig. 9 shows examples of the input, the output of the XPM stage and the output of the regenerator for the two types of input phase noise. Both the constellation and histograms of the sampled phase-value distribution are shown, for a PRBS of length $2^{15} - 1$ impaired by noise with a modulation index of 0.56. This value was chosen to ensure comparability with the experimental results of the previous section. The difference between the two noise distributions is clear from Fig. 9(a). The signal with sinusoidal phase noise shows clear cut-offs of values at $\pm\delta\varphi_{max}$ relative to 0 and π, combined with a tendency of the noisy data points to collect close to the $\pm\delta\varphi_{max}$ values, while the signal with Gaussian phase noise show the characteristic bell shape around both 0 and π. In Fig. 9(b) the two noisy signals have been propagated through the DI and XPM analytically. Again, we see that the XPM output is limited to $0 \le \varphi \le \pi$ when the XPM pump power is adjusted to $2\gamma P_{in} L = \pi$. The signal originally impaired by sinusoidal noise still shows clear cut-offs of the distribution tails. However, due to the mixing of consecutive bits in the DI the noise peaks close to the cut-offs have been re-distributed and the two signals are now in closer resemblance of each other with the exception of the tails. The in principle infinite tails of the Gaussian distribution are now confined to the region $0 \le \varphi \le \pi$ and we see that the 0 and π distributions overlap in the middle. In Fig. 9(c) the two signals have been analytically propagated through the PSA. No re-distribution of noise occurs except for the squeezing of the two distributions of Fig. 9(b). Any data points from the Gaussian distribution on the wrong side of the middle are thus squeezed further away from the original value of the bit. The input signal is impaired by phase noise only and as a result constant amplitude over all bits is seen both at the input and after the XPM stage. At the output however the phase sensitive amplification induces a level of amplitude noise, the distribution of which can be seen in Fig. 9(c) bottom. Notably, the data points collect at the value of maximum amplification (g times the XPM output amplitude) with downwards stretching tails. Again, the sinusoidal noise shows clear cut-offs of the distribution tails, while the Gaussian distribution extends to the value of maximum de-amplification ($1/g$ times the XPM output amplitude). In the DPSK receiver, amplitude and phase both contribute to how the individual bits are received and if an error occurs. Fig. 9(d) shows the sampled distribution of the balanced photodiode output, illustrating how the phase and amplitude distributions of Fig. 9(c) combine in the receiver.

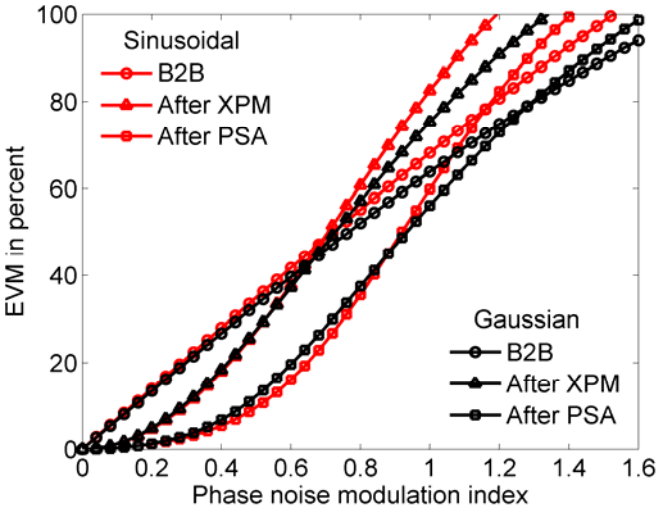

Fig. 10. Optical error-vector magnitude (EVM) as a function of modulation index m for sinusoidal (red) and Gaussian (black) input phase noise distributions, for the signal B2B (circle), after XPM (triangle) and at the output (square).

Fig. 10 shows the optical error-vector magnitude (EVM) [26] as a function of m for each type of phase-noise B2B, after the XPM stage and at the regenerator output. For these simulations the length of the PRBS was increased to $2^{22} - 1$. Compared to the B2B, the XPM output shows improvement in the EVM due to regeneration in the DI for both types of noise, for values of m up to around 0.7. At this point the regeneration is outweighed by penalties due to the aggregation of noise from mixing of consecutive bits. Further regeneration takes place in the PSA with the largest improvement in EVM compared to the B2B seen around $m = 0.5 - 0.6$. The PSA shows improvements in EVM for values of m up to around 1.2 despite the reduced EVM after XPM above $m = 0.7$. Fig. 10 also indicates that the sinusoidal phase noise emulation tends to slightly overestimate the regenerator performance compared to more realistic phase noise, as it results in a larger relative improvement in EVM compared to the Gaussian phase noise. It should be noted that the EVM only serves to quantify the spread of the constellation points from their ideal positions in these simulations. The EVM should not be used as an indicator of the BER performance, especially considering that the main difference between the two noise distributions at all stages are the length of the distribution tails, which will not significantly affect the EVM but will affect the regenerator performance at low BER.

In order to investigate the influence of the difference in distribution tails at low error-rates, the analytical model is applied to theoretically estimate the BER-curves in the

presence of sinusoidal and Gaussian phase noise on the regenerator input. It should be stressed that the analytical model described above is an idealized implementation of the regenerator. While being computationally efficient, it does not capture all aspects of the experiment affecting the BER curves. The model does, however, allow a comparison of how the sinusoidal and Gaussian phase noise distributions affect the BER curves in relation to the most fundamental properties of the regenerator as governed by (1) – (4). At the input to the DPSK receiver, noise loading is implemented by emulating additive white Gaussian noise (AWGN) by adding a phasor with Gaussian distributed noise on both the I and Q components to each bit of the data signal. The bits are then detected in a DPSK receiver comprising a 1 bit DI followed by a balanced photodiode. Different signal-to-noise-ratios (SNRs) are loaded in succession and the resulting number of received errors are counted. The process of generating a noise impaired bit sequence, propagation through (1) – (4), noise loading and error counting in the DPSK receiver is looped until a statistically significant number of errors have been counted for the desired SNR levels, in order to arrive at a BER versus SNR curve.

Fig. 11 shows a set of matching BER curves as a function of the SNR. Curves are presented for a phase noise impaired input signal with sinusoidal (red) or Gaussian (black) phase noise received B2B (solid) and at the regenerator output (open). The employed modulation index is $m = 0.23$. For comparison, a signal without noise received B2B is also presented (blue). Each point on the curves represents up to 5.62×10^{11} simulated bits, and a minimum of 13 errors have been counted for each point to ensure statistical significance [27]. We see that the BER curves for sinusoidal and Gaussian input noise follow each other closely for high BERs. This is consistent with the behavior seen in the EVM analysis. However, at lower BERs we see the B2B penalty for Gaussian noise increase considerably compared to the sinusoidal, and at BER = 10^{-9} the SNR penalty differs by 3.2 dB; an evidence of the long tails on the Gaussian distribution affecting the BER curve. Compared to the B2B curve, the XPM output curve shows reduced penalty for both types of noise for high BERs. However, the penalty for the Gaussian noise increase beyond the B2B penalty at low BERs. A similar trend occurs for the XPM output curve for sinusoidal noise, starting around BER=10^{-9}. The behavior can be understood from the corresponding phase noise distributions, see Fig. 9(a)-(b). As the SNR level is increased by loading lower levels of AWGN at the receiver, the probability of an error is increasingly dominated by the data points closest to $\pi/2$. While phase noise is redistributed through the DI and XPM and most of the data points collect close to the cut-off values at 0 and π, the process also gives rise to tails stretching further towards $\pi/2$ than the B2B distribution, causing the XPM output curve to intersect the B2B curve. For the PSA output BER curves, this behavior is removed for the simulated levels of BER. The phase sensitive amplification is sufficient to straighten the BER curves for both types of noise now coinciding with the B2B curve for a noise free input.

Thus, in relation to the regenerator properties governed by (1) – (4), there exists a region of m where the output of the regenerator is the same for sinusoidal and Gaussian phase noise distributions on the input signal, suggesting that the sinusoidal phase noise may adequately emulate the more realistic Gaussian distributed phase noise. However, the simulations also indicate that the maximum value of m for which BER = 10^{-9} can be reached is lower for Gaussian distributed input phase noise than for sinusoidal. The BER penalty improvements though, are greater for Gaussian than for sinusoidal phase noise due to a larger B2B penalty. It should be noted that according to the analytical model, the experimentally used level of $m = 0.56$ is above the level for which Gaussian phase noise can be regenerated to BER = 10^{-9}. This could indicate that m as calculated from the electrical driving signal in the experiment may be an overestimation of the actual modulation applied to the light in the phase modulator. In the above analysis we have added stochastic errors to the PRBS, implicitly assuming that the errors on consecutive bits are uncorrelated. However, the phase modulator was driven by a single RF tone and correlation can be expected. In order to decrease the correlation, the RF source was unsynchronized compared to the data modulation clock and the RF tones (3.7 GHz, 4.7 GHz or 5.7 GHz) were chosen to prevent the noise and data modulation from being synchronized.

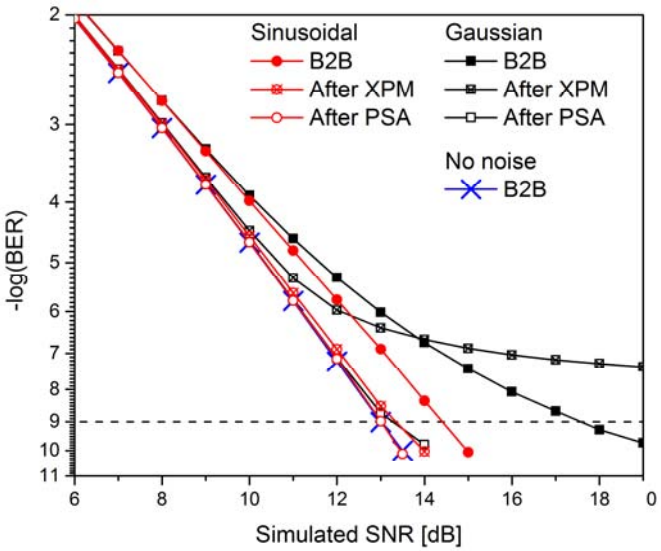

Fig. 11. Simulated BER as a function of SNR between the regenerator output signal and the AWGN loaded at the receiver input. Presented are signals with input sinusoidal (red) or Gaussian (black) phase noise received B2B (solid), at the output of the XPM stage (crossed) and at the regenerator output (open) as well as a signal without input noise received B2B (blue).

VI. Conclusion

We have proposed a scheme for phase regeneration of optical binary phase-shift keying data signals that does not require active phase-locking for phase sensitive amplification. Theoretically, the transfer function of the proposed scheme is observed to converge to an ideal staircase slightly faster than that of the PSA alone, although the differences diminish as the PSA gain increases. The scheme was demonstrated

experimentally for a dual-pump degenerate phase sensitive amplifier. Due to the inherent phase stability of this scheme, a precise dynamic characterization, with a DPSK modulated signal, of the full phase sensitive response in the PSA was possible and a phase sensitive extinction ratio of 12.2 dB was observed. This compares to a 24.8 dB ratio in the static case. The PSA was operated in mild saturation, and the phase sensitive extinction ratio can be increased by reducing the signal power, at the cost of signal OSNR. However, operation at lower levels of OSNR was observed to reduce the BER performance of the regenerator. The proof-of-principle experiment demonstrated phase-regeneration of a 10-Gb/s NRZ-DPSK data signal deteriorated by 3.7, 4.7 and 5.7 GHz phase-noise tones. Receiver sensitivity improvements of up to 3.5 dB are achieved at a bit-error-rate of 10^{-9}. Numerical simulations indicate that the regenerator can operate also in the presence of Gaussian distributed phase noise. Compared to sinusoidal phase noise, the output of the regenerator is found to be comparable also for low BER, although the upper limit on the applicable phase noise strength is reduced while the improvement in receiver penalty is increased due to a larger B2B penalty.

REFERENCES

[1] K. Croussore, C. Kim, and G. Li, "All-optical regeneration of differential phase-shift keying signals based on phase-sensitive amplification," *Opt. Lett.*, vol. 29, no. 20, pp. 2357-2359, 2004.

[2] R. Slavík, F. Parmigiani, J. Kakande, C. Lundström, M. Sjödin, P. A. Andrekson, R. Weerasuriya, S. Sygletos, A. D. Ellis, L. Grüner-Nielsen, D. Jakobsen, S. Herstrøm, R. Phelan, J. O'Gorman, A. Bogris, D. Syvridis, S. Dasgupta1, P. Petropoulos, and D. J. Richardson, "All-optical phase and amplitude regenerator for next-generation telecommunications systems," *Nature Photon.* vol. 4, pp. 690-695, Oct. 2010.

[3] F. Da Ros, D. Vukovic, A. Gajda, K. Dalgaard, L. Zimmermann, B. Tillack, M. Galili, K. Petermann, and C. Peucheret, "Phase regeneration of DPSK signals in a silicon waveguide with reverse-biased p-i-n junction," *Opt. Exp.*, vol. 22, no. 5, pp. 5029-5036, 2014.

[4] J. Kakande, A. Bogris, R. Slavík, F. Parmigiani, D. Syvridis, P. Petropoulos, and D. J. Richardson, "First Demonstration of All-Optical QPSK Signal Regeneration in a Novel Multi-Format Phase Sensitive Amplifier," in *Proc. Eur. Conf. Opt. Commun., (ECOC),* Torino, Italy, paper PDP3.3, 2010.

[5] T. Richter, R. Elschner, and C. Schubert, "QAM phase-regeneration in a phase-sensitive fiber-amplifier," in *Proc. Eur. Conf. Opt. Commun. (ECOC)*, London, U.K., Paper We.3.A.2, 2013.

[6] C. J. McKinstrie and S. Radic, "Phase-sensitive amplification in a fiber," Opt. Exp. vol. 12, no. 20, pp. 4973-4979, 2004.

[7] M. R. Chitgarha, S. Khaleghi, M. Ziyadi, A. Mohajerin-Ariaei, A. Almaiman, W. Daab, D. Rogawski, M. Tur, J. D. Touch, C. Langrock, M. M. Fejer, and A. E. Willner, "Demonstration of all-optical phase noise suppression scheme using optical nonlinearity and conversion/dispersion delay", *Opt. Lett.*, vol. 39, no. 10, pp. 2928-2931, May 2014.

[8] A. Mohajerin-Ariaei, Y. Akasaka, J.-Y. Yang, M. R. Chitgarha, M. Ziyadi, Y. Cao, A. Almaiman, J. D. Touch, M. Tur, M. Sekiya, S. Takasaka, R. Sugizaki, C. Langrock, M. M. Fejer, and A. E. Willner, "Bit-rate-tunable regeneration of 30-Gbaud QPSK data using phase quantization and amplitude saturation," in *Proc. Eur. Conf. Opt. Commun. (ECOC)*, Cannes, France, Paper P.3.20, 2014.

[9] L. K. Oxenløwe, F. Gómez-Agis, C. Ware, S. Kurimura, H. C. H. Mulvad, M. Galili, H. Nakajima, J. Ichikawa, D. Erasme, A. T. Clausen, and P. Jeppesen, "640-Gbit/s Data Transmission and Clock Recovery Using an Ultrafast Periodically Poled Lithium Niobate Device," *J. Lightwave Technol.*, vol. 27, no.3, pp. 205-213, Feb. 2009.

[10] H. C. H. Mulvad, L. K. Oxenløwe, M. Galili, A. T. Clausen, L. Grüner-Nielsen, and P. Jeppesen, "1.28 Tbit-s single-polarisation serial OOK optical data generation and demultiplexing," *Electron. Lett.,* vol. 45, no. 5, pp. 280-281, Feb. 2009.

[11] N. K. Kjøller, K. M. Røge, P. Guan, H. C. H. Mulvad, M. Galili and L. K. Oxenløwe, "A Novel Phase-Locking-Free Phase Sensitive Amplifier based Regenerator," in *Proc. Optical Fiber Commun. Conf. (OFC)*, CA, paper W4C.2, 2015.

[12] M. Matsumoto, "A fiber-based all-optical 3R regenerator for DPSK signals," *IEEE Photon. Technol. Lett.*, vol. 19, no. 5, pp. 273-275, Mar. 2007.

[13] M. Matsumoto, "Fiber-Based All-Optical Signal Regeneration," *IEEE J. Sel. Top. Quantum Electron.* vol. 18, no. 2, pp. 738-752, Mar./Apr. 2012.

[14] P. V. Mamyshev, "All-optical data regeneration based on self-phase modulation effect," in *Proc. Eur. Conf. Opt. Commun. (ECOC),* Madrid, Spain, pp. 475-476, 1998.

[15] A. Fragkos, A. Bogris, and D. Syvridis, "All optical regeneration based on phase sensitive non-degenerate FWM in optical fibers." *IEEE Photon. Technol. Lett.* vol. 22, no. 24, Dec. 2010.

[16] M. Matsumoto, "All-optical DQPSK signal regeneration using 2R amplitude regenerators," *Opt. Exp.*, vol. 18, no. 1, pp. 10-24, Jan. 2010.

[17] G. P. Agrawal, *Fiber-Optic Communication Systems*. 4th ed., John Wiley & Sons, Inc., 2010, pp. 459-510.

[18] I. Kang, C. Dorrer, L. Zhang, M. Rasras, L. Buhl, A. Bhardwaj, S. Cabot, M. Dinu, X. Liu, M. Cappuzzo, L. Gomez, A. Wong-Foy, Y. F. Chen, S. Patel, D. T. Neilson, J. Jacques, and C. R. Giles, "Regenerative all optical wavelength conversion of 40-Gb/s DPSK signals using a semiconductor optical amplifier Mach–Zehnder interferometer," in *Proc. Eur. Conf. Opt. Commun. (ECOC)*, pp. 29-30, Paper Th4.3.3, 2005.

[19] P. Vorreau, A. Marculescu, J. Wang, G. B¨ottger, B. Sartorius, C. Bornholdt, J. Slovak, M. Schlak, C. Schmidt, S. Tsadka, W. Freude, and J. Leuthold, "Cascadability and regenerative properties of SOA alloptical DPSK wavelength converters," *IEEE Photon. Technol. Lett.*, vol. 18, no. 18, pp. 1970-1972, Sep. 2006.

[20] G. P. Agrawal, *Nonlinear Fiber Optics*. 3rd ed., Academic Press, 2001, pp. 260-297.

[21] J. Hansryd and P. A. Andrekson, "Fiber-Based Optical Parametric Amplifiers and Their Applications," *IEEE J. Sel. Top. Quantum Electron.* vol. 8, no. 3, pp. 506-520, 2002.

[22] W. Feller, *An introduction to probability theory and its applications*. 3rd ed., vol. 1, John Wiley & Sons, Inc., 1968, pp. 78-84.

[23] J. P. Gordon and L. F. Mollenauer, "Phase noise in photonic communications systems using linear amplifiers," *Opt. Lett.* vol. 15, no. 23, pp. 1351-1353, 1990.

[24] A. Demir, "Nonlinear Phase Noise in Optical-Fiber-Communication Systems," *J. Lightwave Technol.*, vol. 25, no.8, pp. 2002-2032, Aug. 2007.

[25] A. Mecozzi, "Probability density functions of the nonlinear phase noise," *Opt. Lett.* vol. 29, no. 7, pp. 673-675, Apr. 2004.

[26] R. Schmogrow, B. Nebendahl, M. Winter, A. Josten, D. Hillerkuss, S. Koenig, J. Meyer, M. Dreschmann, M. Huebner, C. Koos, J. Becker, W. Freude, and J. Leuthold, "Error vector magnitude as a performance measure for advanced modulation formats," *IEEE Photon. Technol. Lett.*, vol. 24, no. 1, pp. 61–63, Jan. 2012.

[27] W. Freude, R. Schmogrow, B. Nebendahl, M. Winter, A. Josten, D. Hillerkuss, S. Koenig, J. Meyer, M. Dreschmann, M. Huebner, C. Koos, J. Becker, and J. Leuthold, "Quality Metrics for Optical Signals: Eye Diagram, Q-factor, OSNR, EVM and BER," *in Proc. Int. Conf. Transparent Opt. Netw.(ICTON)*, Coventry, England, Paper Mo.B1.5, 2012.